

High-resolution analytical electron microscopy

One can use elastically and inelastically scattered electrons and x rays from a sample illuminated by an electron beam to determine the composition and structure of extremely small regions of the sample.

R. W. Carpenter

The objective of high-resolution analytical electron microscopy is the determination of the local structure of a wide variety of specimens. This is accomplished by collecting and analyzing the many different signals emitted by a sample when it is irradiated by a highenergy (around 100 keV) electron probe. At present one can determine the structure and composition of solids at spatial resolutions of 50 nm or less; the results are, in general, characteristic of the bulk solids from which the specimens were taken. Such detailed knowledge of the local structure and composition of solids is required especially in geology, materials science, solid-state physics and solid-state chemistry, where properties such as flow stress, fracture modes, electron mobilities and phase transformations are highly sensitive to details of structure and composition.

The basic instrument used for highresolution analytical microscopy is the transmission electron microscope. However, an analytical electron microscope, while retaining the basic characteristics of a transmission electron microscope, is the result of additional instrumentation developments over (approximately) the last ten years. These developments include electron sources and optics that allow formation of very small and very intense electron probes (which therefore have high spatial-resolution), improved vacuum systems to minimize specimen contamination and the addition of various different signal detectors. The challenge is, of course, to do all this while preserving the imaging performance of the instrument.

Analytical signals

The table on page 36 shows the signals most often collected in an analytical electron microscope. The list is not exhaustive, but representative of the methods that are available.

There is also a wide variety of techniques available to collect and display the information produced by these probes.

- ▶ One can form images of the sample directly from the elastically scattered electrons (conventional fixed-beam transmission electron microscopy).
- ▶ One can scan a fine probe across the sample and collect the elastically or inelastically scattered electrons to form an image (scanning transmission electron microscopy).
- ▶ One can produce electron-diffraction patterns from small parts of the sample either by "aperture-selected-area mi-

R. W. Carpenter is professor of engineering and applied science and director of the Facility for High-Resolution Electron Microscopy at the Center for Solid-State Science of Arizona State University.



Advanced analytical electron microscopes.

(a) The photo at left shows a microscope capable of forming either scanned or fixed-beam images. At the top of the column are the field-emission gun and its associated ion pumps: at the bottom of the column is an electron energy-loss specrometer. (Photo courtesy of E. A. Kenik, ORNL.) (b) At right, a dedicated scanning transmission electron microscope. Here the field-emission electron gun and its ion pumps are at the bottom and the electron spectrometer is at the top of the column.

crodiffraction" or by "probe-selectedarea microdiffraction" (also called "convergent-beam microdiffraction").

▶ One can analyze the composition of the sample directly by measuring the energy-loss spectrum of the transmitted electron beam or by observing the spectrum of the x rays emitted by the excited sample.

▶ One can use secondary and backscattered electrons to observe the topography of the sample and to gain some qualitative information on its composition.

The historical development of analytical electron microscopy illuminates the relationship among the various techniques it comprises. From its beginnings in the 1930's, the primary goal of what may be called conventional electron microscopy has been high image resolution, that is, determining the geometric arrangement of atoms relative to one another in solids: determining the identity of these atoms was a secondary objective. This goal required that electron optics for imaging be given preference in instrument design. Energy-loss spectroscopy was first proposed as an analytical method in 1944, but inadequate vacuum systems and other instrumentation problems delayed its widespread use for more than two decades.1 X-ray spectroscopy began to attract increasing interest when solid state detectors capable of fast parallel data collection were first coupled to transmission electron microscopes.2 Convergent-beam diffraction was first demonstrated about forty years ago, but only recently, with the advent of suitable lenses in

clean vacuums, has the technique been useful for analytical electron microscopy.³ A major stimulus for developing lenses and field-emission sources capable of forming the small probes that are necessary for high-spatial-resolution microanalysis and microdiffraction came from research on forming scanned transmission images, for which the resolution is dependent on the size and current density of the incident probe.⁴

All of these methods have been used more or less independently for research. Recently developed instruments make it possible to use them all in a single instrument, in some cases simultaneously. Two typical analytical electron microscopes of advanced design are shown in figure 1. Figure 1a shows an electron microscope fitted with a field-emission gun that can form either conventional or scanned transmission images (TEM/STEM/FEG). Figure 1b shows a dedicated scanning transmission electron microscope (D-STEM) also fitted with a field-emission gun. The principal difference between the two is in the way they form their D-STEM instruments form scanned images exclusively.

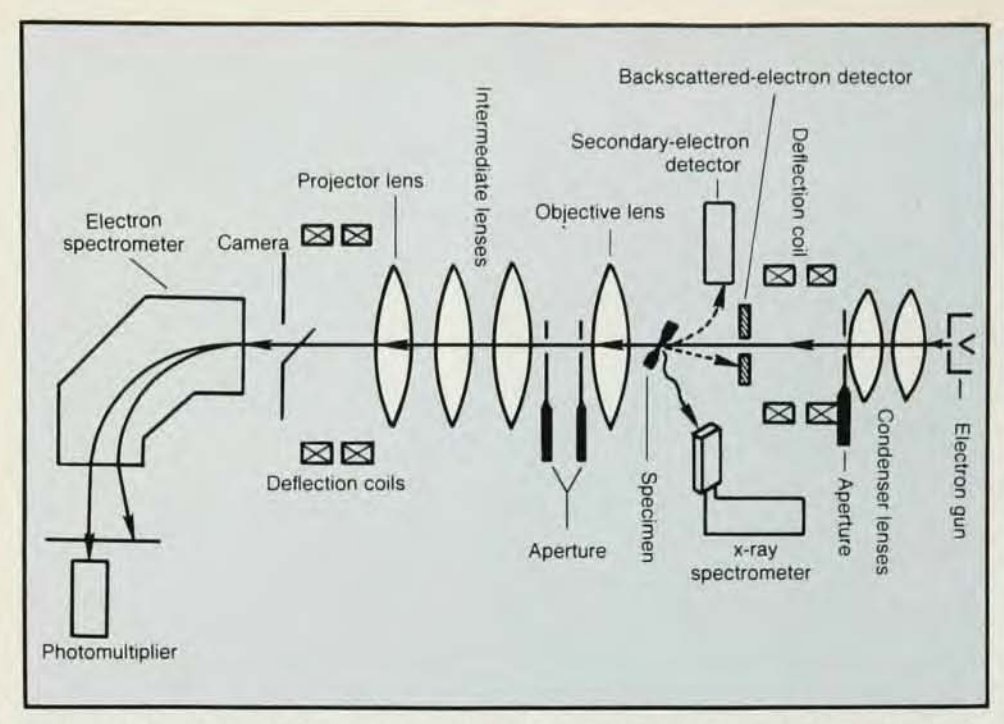
Modern instrumentation

Figure 2 shows schematically the operating parts of a modern analytical electron microscope. It has three major components in common with all electron microscopes: the illumination system, the objective-lens-specimen-stage system and the magnification-lens-camera system. In addition, there are several sets of scanning coils,

two spectrometers for measuring the energy distribution in the emitted x-ray spectrum and in the transmitted electron beam, and detectors for secondary and back-scattered electrons. These components are shown in their correct positions relative to the electron source and the specimen.

The most prominent feature distinguishing an analytical electron microscope from a conventional one is the ability to form small electron beams for the incident probe, which is necessary for microelemental analysis, microdiffraction and scanned-image formation. The probe is usually formed by an objective lens of the condenserobjective type, which can operate in two different modes: In the "microprobe" mode, the lens is strongly excited and that portion of its magnetic field on the electron-entrance side of the specimen (the "pre-field") focuses a convergent microprobe on the specimen, while in the "conventional" mode the effective lens field is weaker, and a larger (diameter more than 250 nm), nearly parallel beam illuminates the specimen. A microscope fitted with an objective lens of this type together with scanning coils and various signal detectors allows experimenters to use on a single suitable specimen all the imaging, diffraction and microanalysis methods mentioned above.5,6

Electron sources and vacuum systems have important but less obvious effects on the performance of electron microscopes. The lenses of the illumination system demagnify the electron source to form a small probe at the specimen; because electrons are lost



Components of an analytic electron microscope such as the one shown in figure 1a. It can provide analyses of local composition and structure such as those shown in figure 3.

from the probe during demagnification, the brightness of the image is reduced. Field-emission electron sources are being increasingly used in advanced analytical microscopes because they are much brighter than the familiar tungsten thermionic sources of conventional electron microscopes. Furthermore the effective electron-emitting region of a field emission sources (generaly less than 10 nm in diameter) is much smaller than the corresponding region of thermionic sources, which are typically 10 microns or more in diameter. The field-emission sources thus produce current densities higher by about a factor of 1000 than those achieved by thermionic sources.7

Field-emission sources were first developed for scanning transmission microscopes, where their characteristic high brightness is necessary to form high-resolution images. For the same reason one can also expect the best results in microdiffraction or microelemental analysis at the small-probe spatial-resolution limit when one uses field-emission sources. The brightness of field-emission sources is also useful in high-resolution conventional imaging experiments: It permits a reduction in the time required for recording the image (the photographic exposure) from 3 or 4 seconds to about 0.5 second, which decreases the probability that the image will be disturbed by mechanical or electrical instabilities in the microscope. Field-emission sources require an ultrahigh vacuum for stable operation, particularly in the source chamber; however, an analytical electron microscope also requires ultrahigh vacuum for reasons beyond field-emission stability.

Observations in many laboratories have shown that the vacuum environment in conventional electron microscopes is not "clean" enough for analytical purposes. The major problem is contamination of the irradiated specimen area. The usual contamination, called "system contamination," consists of amorphous deposits of carbonaceous material on both surfaces of the electron-transparent specimens in regions irradiated during microprobe experiments; they arise from organic compounds that diffuse on the specimen surface to where the incident probe is focused and are there decomposed to amorphous carbon. These deposits form rapidly in poor vacuum environments whenever the sample is illuminated with a microbeam.8 Contamination will degrate scanning transmission images and microdiffraction patterns and will obviously interfere with microelemental analysisespecially if carbon analysis is required.

Conventional vacuum systems in-Methods for structural analysis

Primary information

Signal

Transmitted electrons elastic direct beam bright-field images Bragg-scattered dark-field images direct plus Bragg high-resolution images and microdiffraction patterns microanalysis of light inelastic elements (Z ≤ 30) energy-loss images Emitted x rays microanalysis of medium to heavy elements (Z ≥ 12) characteristic x-ray images

volving oil-diffusion and rotary mechanical pumps are inadequate either to stabilize the field-emission sources or to avoid sample contamination. Microscope designers have responded to these problems by gradually adjusting their designs to incorporate ultrahigh vacuum technology, but the process has been evolutionary rather than revolutionary and it is not complete. At present, commercial instruments incorporate ion pumps to stabilize their field emission sources and ion pumps or advanced liquid-nitrogen traps to clean their specimen chambers. These instruments attain residual pressures of roughly 10-8 torr at the specimen and less than 10-10 torr in their gun chambers-a significant improvement relative to the roughly 10⁻⁵ torr attainable in conventional electron microscopes. System contamination generally remains within manageable limits if the pressure within the specimen chamber is kept below 10-8 torr for most experi-However, laboratory-conments. structed instruments have produced results in the analyses of surface structures-concerning observations of dislocation intersections with free surfaces and surface-structure phase transitions-which show that further improvements are possible.9 We may expect that many future instruments will be true uhv systems.

Microelemental analysis

Figure 3 illustrates the versatility and range of an analytical electron microscope, in this case applied to a structural ceramic. The bright-field transmission image shows a polycrystalline region of sintered silicon nitride fluxed with magnesium oxide. This material is not in thermodynamic equilibrium after sintering and contains a number of different phases, some of which are noncrystalline. The variability of the composition is shown by the electron energy-loss spectra and energy-dispersive x-ray spectra shown for the regions marked by A to D in the image. The microdiffraction patterns from the same areas demonstrate the structural differences between them. The energy-loss spectra show peaks corresponding to excitations of innershell electrons for elements in each phase superimposed on a background that decreases rapidly with increasing energy loss. The corresponding energy-dispersive x-ray spectra show characteristic emission peaks for K-series x rays from the (heavier) metallic elements in the four regions on a low background that varies slightly with

At present, energy-dispersive x-ray spectroscopy is a more highly developed and simpler method for microanalysis. However, the higher sensitivity of energy-loss spectroscopy for Cry.o.tron.ics (krī'ə trań iks) n. A combination of expertise in cryogenic temperature generation and electronic detection, measurement, and control. Identifies a source of fast, stable, accurate, state-of-the-art low temperature refrigeration systems and equipment.... as in 'Lake Shore Cryotronics'.'

Lake Shore defined "Cryotronics" over a decade ago. And we've been refining it ever since, through continual technological innovation in cryogenic products. Today Lake Shore Cryotronics provides state-of-the-art sensors, instrumentation, dewars, closed-cycle and continuous flow refrigeration systems . . . along with calibration and custom engineering services . . . for virtually every cryogenic application.



New DRC-80C Controller



CT-310 Cryotran System



GR-200 Germanium Sensors

These are only a few of the many Lake Shore products which can help you. So when your needs call for the defined leader, come to Lake Shore . . . we know cryogenics COLD!

Cryogenic Thermometry • Instrumentation • Systems
Calibrations • Dewars



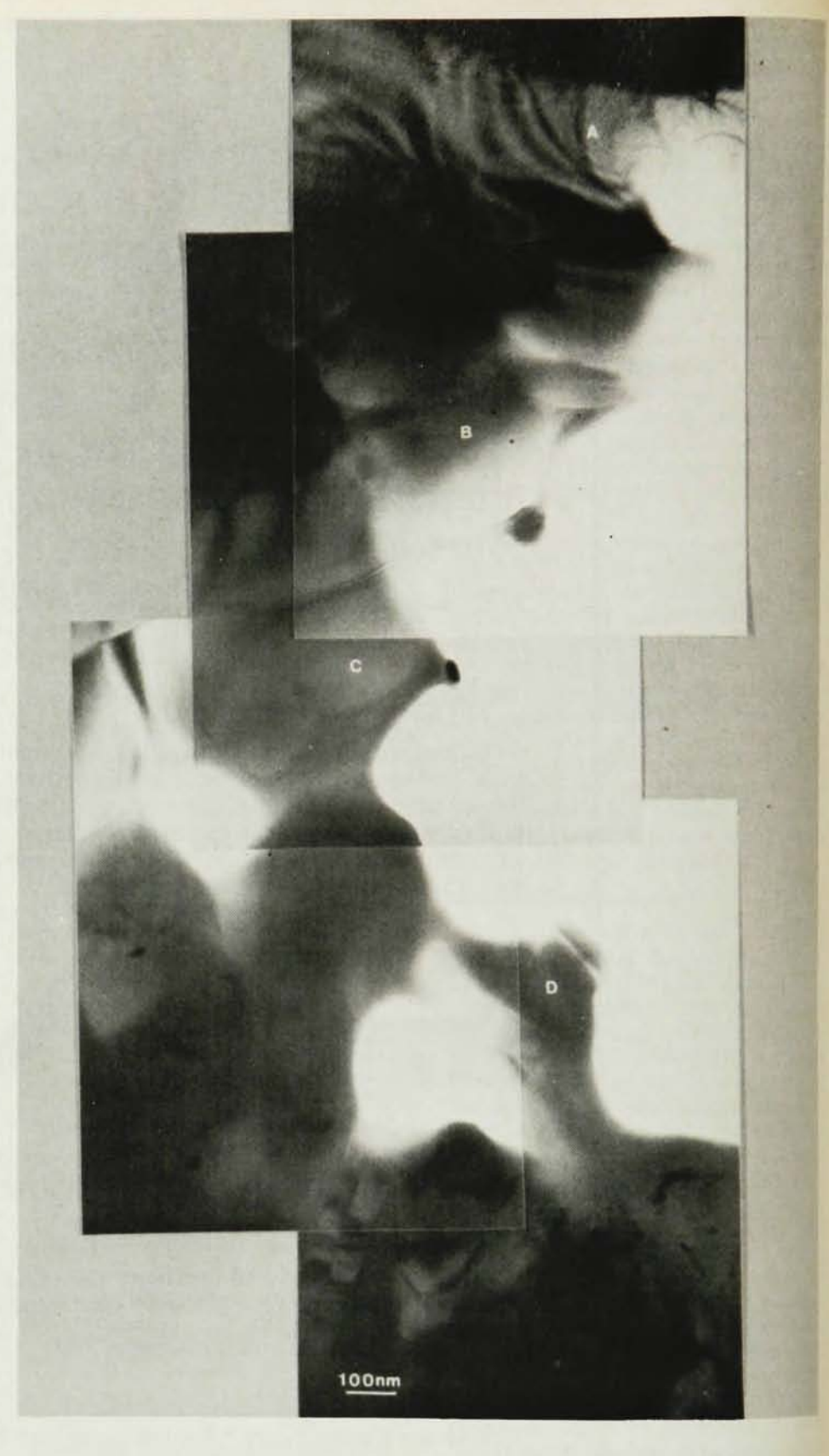
64 E. Walnut St., Westerville, OH 43081 • (614) 891-2243 In Europe: Cryophysics: Oxford • Versailles • Darmstadt • Geneva In Japan: Niki Glass Co., Shiba Tokyo light elements and its higher energy resolution are the basis for active and growing research on the method. The measured count rate in a characteristic x-ray spectrum peak, for example a K_{α} -peak, is given by

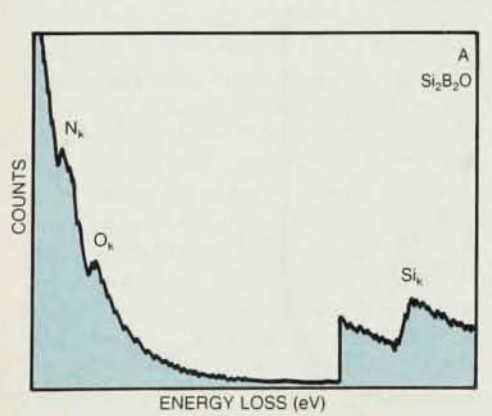
$R_x = Q \operatorname{Jnuf} E$

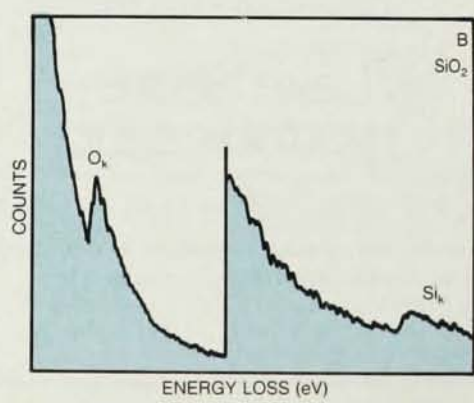
where Q is the K-shell ionization cross section, J the incident electron flux, n the volume concentration of the atom of interest, w the K-shell fluorescence yield for the excited atoms, f the fraction of the total K-shell emission that is in the K_{α} peak and E the detection efficiency. The fluorescence yield, that is, the probability that a K-shell ionization will decay via its characteristic xray emission, depends on Z, the atomic number of the target atoms, and is very small for low-Z elements. The complementary decay process, Auger emission, has probability 1 - w and is larger for low-Z elements. However, because the escape depth of Auger electrons is small, they are not useful for internal microanalysis.

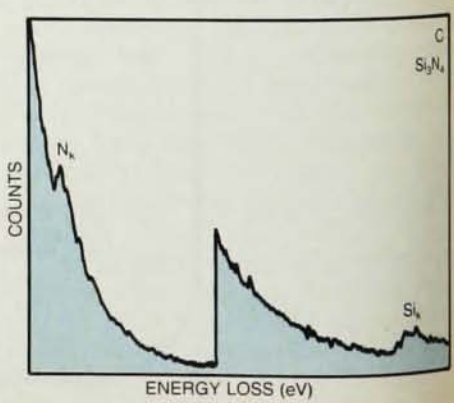
The variation of fluorescence yield with atomic number is an important point and is one of the reasons that both x-ray and electron spectrometers are used on analytical microscopes. For x-ray energy-dispersive spectroscopy one uses lithium-drifted silicon solidstate detectors having an area of 10 to 30 mm² and generally located about 1 cm from the specimen. Low-energy x rays are absorbed in the beryllium windows, gold layers and silicon dead layers of these detectors while those of higher energy are not. The geometric collection efficiency is relatively low for all characteristic x rays because they are emitted from the irradiated specimen with radial symmetry, while the solid angle subtended by the detector at the specimen is typically around 0.1 steradian.

In the case of electron energy-loss spectroscopy, on the other hand, every K-shell excitation results in a loss-electron, with the magnitude of the energy loss equal to the ionization energy of the target atom. These inelastically scattered electrons are scattered through small angles, so the distribution is strongly peaked about the for-



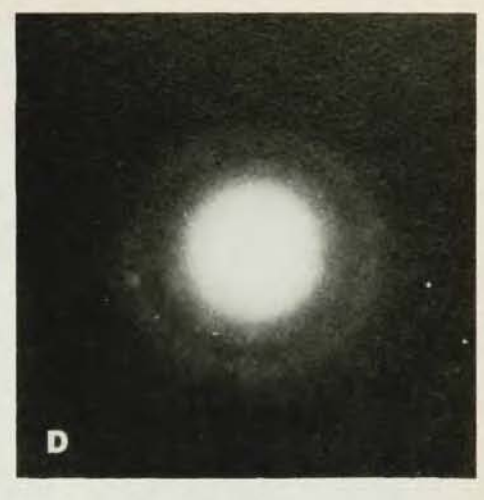






Structure and composition of small regions of a sample of sintered silicon nitride, shown in the superposed photos opposite. The spectra and diffraction patterns come from the spots labelled A–D: at right, convergent-beam diffraction patterns from aras A and D; below left, electron energy-loss spectra from all four regions; below right, x-ray energy-dispersive spectra. The sample is highly inhomogeneous in composition and structure, for example, it is crystalline at A, B and C, and amorphous at D. Figure 3





ward scattering direction. A properly designed and operated energy-loss spectrometer will therefore have a detection efficiency near unity. The count rate from a K-shell ionization edge is then

$$R_E = JnQ(\alpha, \Delta E)$$

where J is the flux, as before, n is the number of ionized atoms and $Q(\alpha, \Delta E)$ is the partial ionization cross section for a spectrometer acceptance angle α over the energy-loss range ΔE at the edge with the characteristic loss energy E. 10

The x-ray energy-dispersion and electron energy-loss methods are complementary: Each has advantages and both are necessary for a complete characterization of the elements in a specimen.

Energy-loss spectroscopy is the less familiar of the two methods, and a simple description of the various regions of an experimentally acquired spectrum may be useful here. Figure 4 shows an energy-loss spectrum for a thin carbon foil and extending from the zero-loss peak (the direct beam, marked A) to beyond the K-shell excitation edge at 283 eV. The peak marked B, at a loss of 24 eV, corresponds to a single plasmon or valence electron excitation; C and D mark simple increases in detector amplification. The sharp jump at 283 eV corresponds to excitation of K-shell electrons, and the small broad peak following the K edge is a result of a convolution of the plasmonloss and the K-loss peaks. We can

arbitrarily divide the spectrum into three regions:

- ▶ the zero-loss peak, which includes unscattered electrons and quasi-elastically scattered electrons (scattered by phonons)
- ▶ the low-loss region extending from about 5 to 50 eV, which includes plasmon and valence-electron scattering
- ▶ the inner-shell-loss region, which has a useful range from around 100 to 3000 eV.

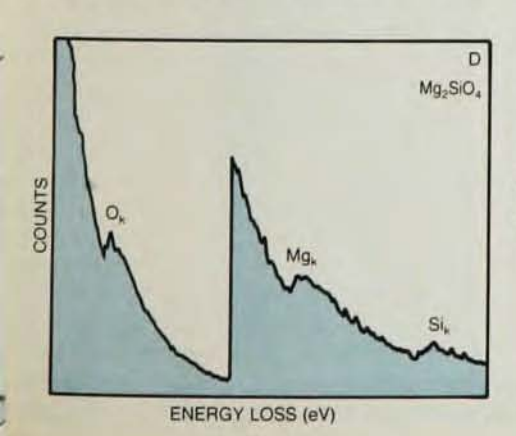
All but a few percent of the electrons in the spectrum are in the zero- and plasmon-loss regions, and the small innershell peaks ride on a large, continuously decreasing background.

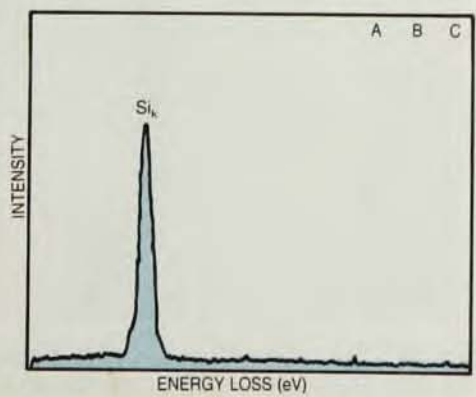
Both the plasmon-loss and the innershell-loss peaks shift their positions in alloys with changes in the chemical composition; however, the plasmon shifts are, in general, very small and correlation of the peak shifts with changes in the composition of the specimen is difficult.11 For this reason, one prefers inner-shell losses for microanalysis. The spectrometers used for energy-loss microanalysis are most often of the magnetic-sector type with a dispersion of about 4 microns/eV. An energy resolution between 5 and 15 eV is suitable for microanalysis. The loss spectrum is scanned across a scintillator-photomultiplier detector and recorded serially with a computer or multichannel analyzer.

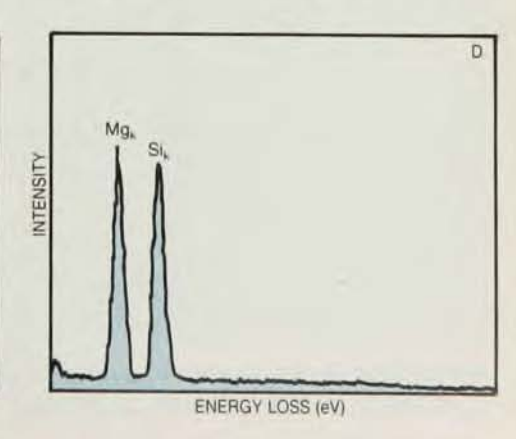
Two important quantities that determine the usefulness of the x-ray and electron spectroscopies are the "mini-

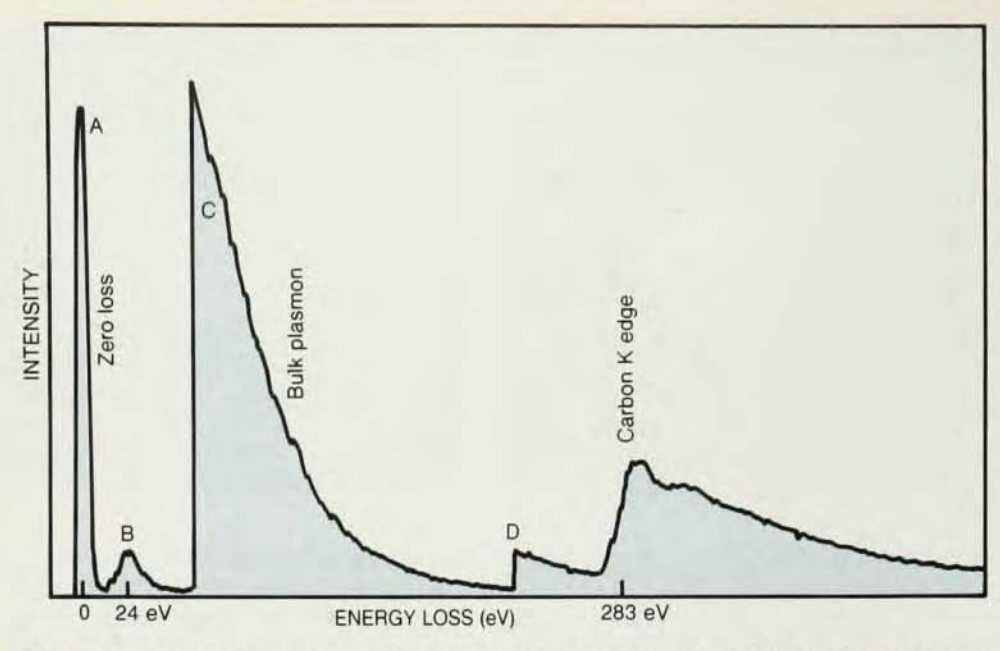
mum detectable mass" and "minimum detectable mass fraction." The minimum detectable mass refers to the smallest detectable amount of some element in the specimen in a free or pure state or in a weakly scattering matrix. It is a measure of the sensitivity of the system, and "clean" spectra free of system artifacts are necessary to make it as small as possible. The minimum mass fraction refers to detection of some element in a surrounding matrix that may not be weakly scattering, so that the background from the matrix becomes the limiting factor. Methods for calculating and measuring these quantities have been considered in detail elsewhere. 12,13 Both depend on the operating mode of the microscope, the accelerating voltage, and the atomic numbers of the elements in the target and the thickness of the target. In general, for optimized systems the minimum detectable mass will be between 10-18 and 10-20 grams and the minimum detectable mass fraction will be in the range of 0.1 to 3%.

The development of quantitative methods to determine local compositions from x-ray or electron spectra taken from thin specimens is currently the primary objective of microanalysis research. Such quantitative methods are most developed for x-ray energy-dispersive spectra taken from homogeneous (single-phase) specimens. The methods are based on a comparison of the integrated intensities of the characteristic peaks—after subtraction of









Electron energy-loss spectrum from a thin film of amorphous carbon (120 keV incident beam energy): A is the zero-loss peak; B corresponds to a single plasmon excitation; C and D are amplifier resettings. K-shell electrons are excited at 283 eV. Figure 4

the background and corrections for atomic-number dependence. To convert the peak-intensity ratios to concentrations, one can use either standards of known composition or calculations of the cross-sections.14,15 The table on page 41 is an example of the accuracy obtainable with energy-dispersive spectroscopy; it shows a comparison of compositions obtained with a "thin-film standardless" spectroscopic method with compositions obtained with an independent bulk chemical analysis.14 The agreement between the two methods was good, particularly for the determinations made with Kshell characteristic emission peaks. Excitation cross-sections for L- and higher-shell emission peaks are less well known at present.

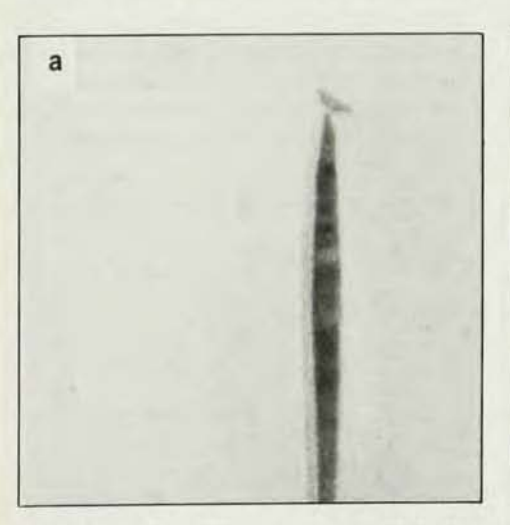
The quantitative methods currently available for energy-loss spectra enable one to make microanalytic measurements for light elements in thin specimens with an accuracy of about \pm 15% from an analysis of the peaks from K-shell excitations. The most important sources of uncertainty in the analysis are the angular and energy dependence of the partial ionization cross section, $Q(\alpha,\Delta E)$ and the effects of multiple inelastic scattering on the loss spectrum.

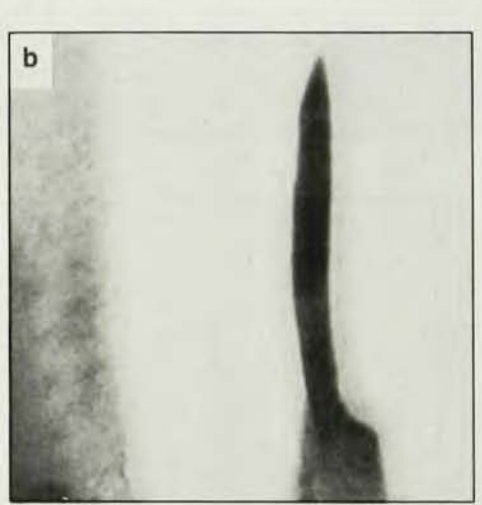
To calculate the elemental composition from the electron energy-loss spectra one uses a single-scattering treatment of inelastic scattering. This is a standard approximation of thin-foil microscopy; its validity depends on the thickness of the specimen in the particular situation of experimental interest. The effects of specimen thickness on the shapes of electron-loss are simple to recognize experimentally: As the thickness increases, the intensity of the plasmon-scattering peak increases

relative to the intensity of the zero-loss peak, and the inner-shell excitation peaks become difficult to detect above the increasing background intensity. Furthermore, the relative intensity of the inner-shell energy-loss peaks from different constituents of multielement specimens changes rapidly beyond a limiting thickness value, producing an apparent change in composition with thickness. Experimental results suggest that the apparent compositional changes due to multiple scattering are within the uncertainty limits of the analysis if one obtains spectra for regions of the specimen thinner than about 20% of the mean free path of plasmons. 17 One can easily find acceptable regions by observing the relative intensities of the first plasmon peak and the zero-loss peak: The ratio is proportional to the thickness of the specimen. For typical plasmon mean free paths, these regions correspond to specimens 20 to 70 nm thick.

One must also restrict specimen thicknesses to this range or less to achieve maximum spatial resolution with energy-dispersive spectroscopy. This is a particularly important problem when one examines specimens containing local heterogeneous regions such as interfaces or particles of a second phase. Figure 5 and the table next to it (on page 41) illustrate the large differences in apparent composition that can occur as a result of different experimental conditions.14 With small particles of precipitates, beam spreading can be a problem; at present, the best solution to this problem is making an extraction replica, but one must be careful to avoid chemical changes in the extractant while preparing the specimen. Small particles containing only about 10-18 gram of material have been analyzed using this method.18

Microanalysis based on energy-dispersive spectroscopy has a reduced spatial resolution in thick foils, probably





C

Precipitates from a sample of austenitic stainless steel. Each photo shows an area about 200 nm across. The table on the next

page shows detailed analyses of the M₂₃C₆ precipitates shown in these photos, as well as of the steel matrix. Figure 5

because of multiple elastic scattering of incident electrons within the foil, which causes an increase in the volume from which x rays are emitted. In electron-transparent foils of heavier metals, such as copper or gold foils about 100 nm thick, the x-ray emission region is several hundred nanometers in diameter. The small, high-current-density probes that the field-emission sources produce are useful for high-spatial-resolution microanalysis only for thin specimens.

The reader interested in using highresolution analytical microscopy should not view these restrictions on specimen thickness as an unnecessary burden: It has been known for some time that clean, thin specimens (less than around 50 nm thick) are necessary for quantitative interpretation of highresolution images; this requirement is uniform for all the experimental techniques we have discussed. The restriction on specimen thickness can be relaxed to some extent if one uses incident electrons with a higher energy. Exploratory experiments and calculations by a number of investigators have shown that peak-to-background ratios in microelemental analyis, spatial resolution and high-resolution images are all improved in thicker specimens with high-voltage microscopes (with accelerating voltages generally up to 1 MV, but higher in a few cases). Only high-resolution microscopes have been designed for high-voltage operation thus far.

Microdiffraction

Microdiffraction and imaging in an analytical microscope are extended beyond the capabilities found in conventional electron microscopy. The ability to form small probes and the low specimen contamination rate in an analytical instrument allow one to perform interesting and useful diffraction experiments with what is called "convergent-beam electron diffraction." Here one selects the diffracting volume by focusing the incident probe on the appropriate part of the specimen: The diameter of the probe and the thickness of the specimen determine the volume. One can obtain probe sizes down to 0.5 nm in analytical microscopes fitted with field-emission sources. For a typical incident probe of 5 nm diameter and a specimen 30 nm thick, the irradiated volume contains approximately 104 atoms.

One can obtain diffraction patterns from very small sample volumes with instruments that cannot form small, convergent probes by using small apertures to select an area of the sample. This "aperture-selected-area microdiffraction" is restricted to a minimum diameter of about 250 nm, corresponding to an irradiated volume containing

Comparison of microanalytic methods

Sample	Incident Energy (keV)	Measured Intensity	Composition (w	eight percent) Bulk
β-NiAl	200	Ni-K/Al-K = 2.05	Ni = 69.5	Ni = 68.5
	100	Ni-K/Al-K = 1.79	AI = 30.5 Ni = 69.6 AI = 30.1	Al = 31.5 Ni = 68.5 Al = 31.5
β-ZrNb	200	Nb-K/Zr-K = 0.163	Nb = 14.9 $Zr = 84.0$	Nb = 15.4 Zr = 84.6
β-CuZn	100	Cu-K/Zn-K = 1.63	Cu = 60.4 Zn = 39.6	Cu = 60.2 Zn = 39.8
Ni ₄ Mo	120	Mo-K/Ni-K = 0.113	Mo = 29.2 Ni = 70.8	Mo = 29.0 Ni = 71.0
	120	Mo-L/Ni-K = 0.246	Mo = 27.4 Ni = 72.6	Mo = 29.0 Ni = 71.0
NbHf	120	Nb-L/Hf-L = 1.30	Nb = 43.9 Hf = 56.1	Nb = 45.9 Hf = 54.1
Fe-13 Cr-40 Ni	120	Fe-K/Ni-K = 1.25	Ni = 40.1 Cr = 14.2	Ni = 40.4 Cr = 13.2
	120	Cr-K/Ni-K = 0.426	Fe = 45.7	Fe = 46.6
Fe-13 Cr-20 Ni	120	Fe-K/Ni-K = 3.59	Ni = 20.0 Cr = 14.5	Ni = 19.7 Cr = 13.3
	120	Cr-K/Ni-K = 0.0880	Fe = 65.5	Fe = 66.9

perhaps 10⁸ atoms. For this reason diffraction patterns formed with convergent beams are more sensitive to local changes from composition gradients or lattice defects than aperture-selected microdiffraction patterns.

A unique and less obvious feature of convergent-beam patterns is that they contain information on three-dimensional configurations. The patterns are formed by irradiating the specimen with a focused probe of electrons; the convergence half-angle of the beam is usually in the range 6-15 milliradians, which is large compared to the nearly parallel beams used for aperture-selected-area diffraction. Because of the angular spread of the incident electrons, the Bragg condition can be satisfied for reflections in reciprocal-lattice planes that lie above the plane containing the lattice origin, the so-called "higher order Laue zones." If we denote the lattice planes by their usual Miller indices, (h k l), then diffraction vectors corresponding to higher-order reflections satisfy

$$[u\ v\ w]\cdot (h\ k\ l) = n$$

where n is a positive integer and $[u \ v \ w]$ is a vector antiparallel to the axis of the incident beam cone of electrons. For

"zero-layer" reflections n=0. The diffraction vector components along the incident beam direction for higher-order Laue zones carry structural information along the beam direction in addition to the usual two-dimensional information present in the pattern.

The two patterns shown in figure 6 illustrate the use of upper-layer diffraction to examine properties of crystals. The dark lines in the central discs result from excitation of Bragg reflections from higher-order Laue zones whose indices shown in figure 6a.

One can obtain quite detailed information about the crystal structure from such patterns. When the irradiated crystal volume contains a dislocation, for example, all upper-layer lines corresponding to Bragg diffraction planes distorted by the displacement field are split into fringes. Kikuchi lines corresponding to upper-layer Bragg reflections exhibit the same behavior. (Kikuchi lines arise from Bragg diffraction of inelastically scattered electrons.) Because the diffracting volume is small relative to the extent of the defect displacement field in the lattice, the effect is easily observed, and the Burgers vector (which describes the magnitude and direction of the crystal disloca-

Analysis of precipitates

Element	Composition (weight percent)						
	Extracted precipitate (figure 5a)	Suspended precipitate (figure 5b)	precipitate (figure 5c)	Matrix			
Sn	0.05	2.3*	1.1	1.3			
Mo	16.7	14.2	8.7	3.9			
Cr	65.9	58.2	30.9	18.4			
Mn	0.05	0.2	1.47	1.5			
Fe	14.6	21.6	47.9	62.3			
Nn	2.8	3.6	10.0	12.6			

^{*}Increased silicon content probably due to the heavy contamination layer surrounding the precipitate.

Swagelok

for trouble-free connections in tube or pipe systems from 1/16" to 2" O.D.

SWAGELOK Tube Fittings are available from local distributor stocks in stainless steel, steel, brass, aluminum, nylon, TFE and other machineable metals and plastics. This general guide to the complete SWAGELOK product line will help you select specific designs to meet your service requirements.

CRAWFORD FITTING COMPANY

29500 Solon Road, Solon Ohio 44139 Crawford Fittings (Canada), Ltd., Ontario

©1981 MARKAD SERVICE CO., all rights reserved C-56

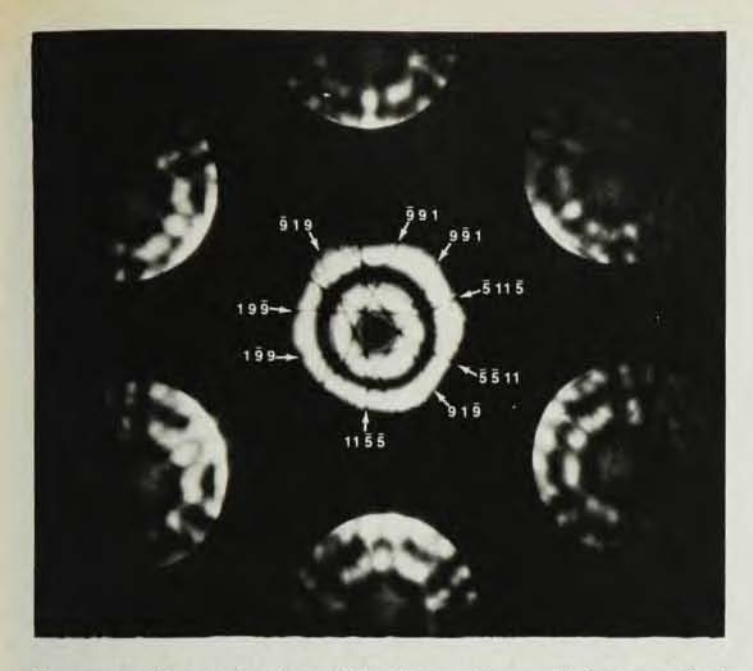




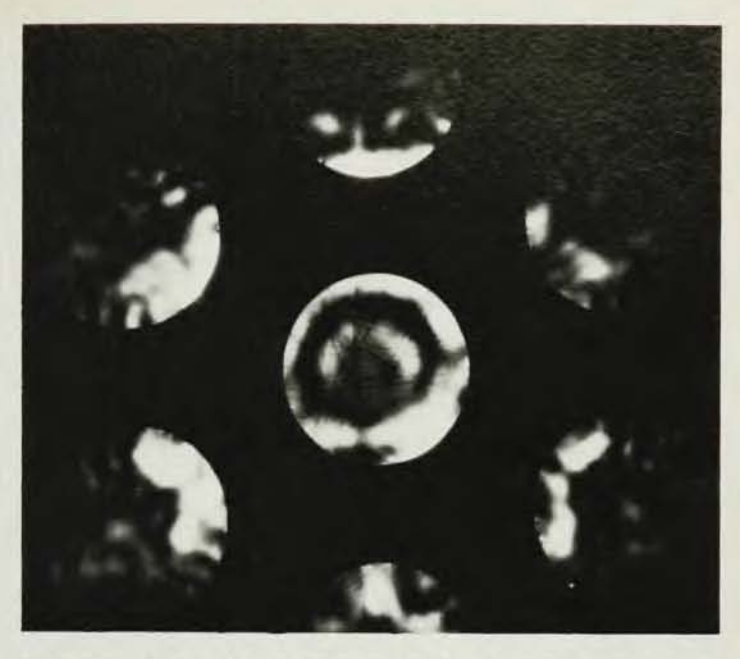




FEMALE CONNECTOR



Convergent-beam electron-diffraction patterns: (a) from a perfect crystal, with "upper-layer lines," from the indicated crystal planes; the



outer disks are all of the |2 2 0 | type; (b) from a crystal that having a dislocation with Burgers vector $\frac{1}{2}[0\ \overline{1}\ 1]$. Figure 6

tion) can be determined from the splitting symmetry of both upper-layer and Kikuchi lines.19 The upper-layer lines exhibit high sensitivity to local lattice distortion, and it is therefore reasonable to expect that their positions within the central disc depend on local lattice-parameter changes caused, for example, by a concentration gradient. This is indeed so, and differences in local crystal lattice parameter can be determined20 with an accuracy of about 1 part in 500. This method of detecting fluctuations in local compositions from shifts of upper-layer lines is complementary to the microanalysis methods; the line shifts give no direct information concerning the chemical identity of the atoms causing the lattice distortion, but the diffraction method is likely to have higher spatial resolution in all but the thinnest crystals.

One can also use upper-layer diffraction effects in convergent-beam diffraction patterns to determine crystal symmetry. An elementary example is available in figure 6. Note that the array of upper-layer lines from the perfect crystal has three-fold rotational symmetry about the incident beam direction, but the symmetry of the zerolayer Bragg spots (the six large spots from the [220] reflections) alone indicates six-fold symmetry about the [111] axis. The true symmetry of the perfect crystal axis is given when threedimensional information is contained in the diffraction pattern. The relationship between convergent-beam diffraction and three-dimensional crystal symmetry can be used efficiently to identify the structure of complex materials.21 This technique is very effective when used with microanalysis to identify small second-phase particles that occur in many materials such as semi-

conductors or steels. When one uses very small probes from field-emission sources (less than about 0.5 nm in diameter) for convergent-beam diffraction, one observes coherent interference effects in high-divergence patterns. These interference effects have been observed in regions where the Bragg spots (really disks) overlap, and in convergent-beam shadow images. The effects are the diffraction analogues of fringe imaging in high-resolution lattice or structure images in conventional or scanning transmission electron microscopy. They promise to yield structural information at higher resolution than the imaging modes22 and they offer intriguing possibilities for examination of local lattice distortions associated with segregation to lattice defects or nucleation phenomena.

Imaging

A variety of imaging modes is avail-

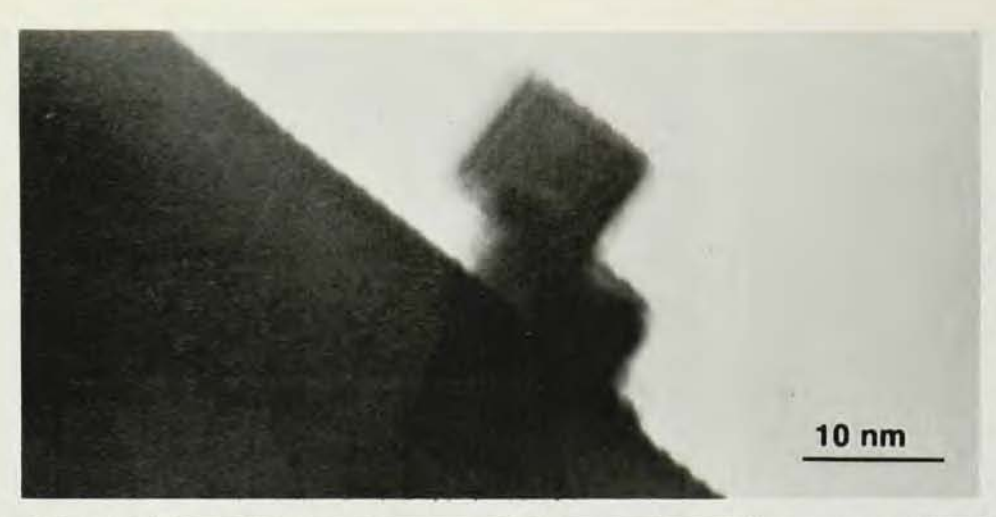
Acronyms

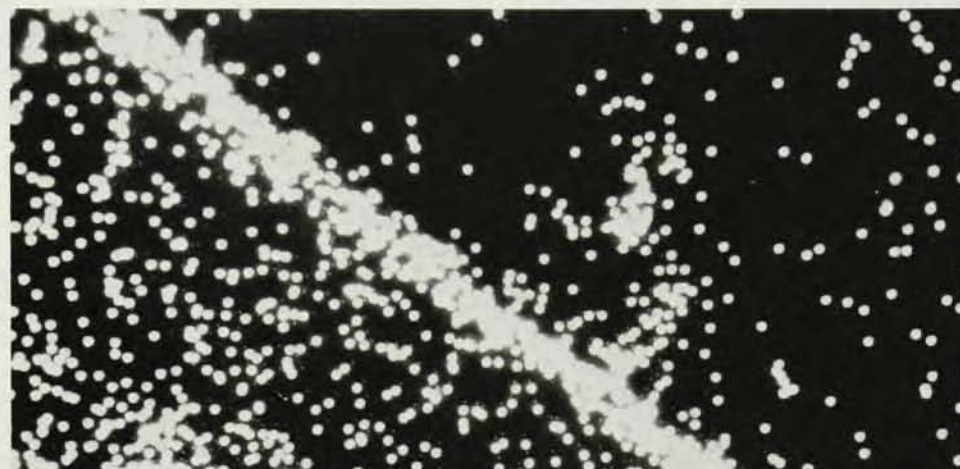
Researchers in analytical electron microscopy use many acronyms; among the most common are:

AFM analytical electron microscopy CBED convergent-beam electron diffraction (X)EDS (x-ray) energy-dispersive spectroscopy (E)ELS (electron) energy-loss spectroscopy HOLZ higher-order Laue zones **HVEM** high-voltage electron microscope MDM minimum detectable mass MMF minimum (detectable) mass fraction SAD (aperture-)selected-area microdiffraction STEM scanning transmission electron microscopy ("conventional" or "fixed-beam") TEM transmission electron microscopy ultrahigh vacuum

able in analytical electron microscopes. The most widely used, of course, are conventional, or fixedbeam, and scanning transmission images. The resolution attainable by either method is in principle the same, because of reciprocity. The point-resolution limit at optimum defocus for high-resolution analytical microscopes is calculated to be slightly less than 0.3 nm (at 100keV) for either fixed-beam or scanned images, and experiments have nearly reached the limit. Four years ago the best conventional microscopes dedicated to high-resolution research did not have as high a resolution,23 and present dedicated high-resolution microscopes perform with only slightly better resolution. Taking into account the fact that the x-ray spectrometer is mounted close to the objective lens and that the specimens can still be tilted approximately ± 20°, these instruments are a noteworthy achievement for the engineers and designers who built them. With such instruments one can examine the relationship between structure and elemental segregation nearly at the atomic level. These new instruments are responsible for the rapidly increasing interest in analytical electron microscopy.

In practice there are important differences in conventional and scanned bright and dark field images, particularly for crystalline specimens. Fixed-beam images are recorded in parallel (all at once, on photographic film), and scanning images are recorded serially (with photomultipliers or solid-state detectors). With instruments fitted with field emission guns, both methods produce excellent results at medium resolution. ¹⁸ At high resolution, fixed-beam images are clearly superior to scanned images at present. ²² However, because





Cubes of magnesium oxide covered with a thin layer of evaporated nickel. At top is a bright-field scanning electron image, below is an image formed from nickel K_{α} x rays, clearly showing the nickel layer. (Research of Perter Turner, Giffith University, Autralia.) Figure 7

scanned images are formed by modulating the intensity of a display tube with some signal from the specimen as the small probe scans over it, one can think of using signals other than elastically scattered electrons. Some experimenters have used characteristic x rays from some atomic constituents of the specimen to form low resolution "x-ray scanning images." With analytical microscopes fitted with field-emission guns, one can form high-resolution images with either characteristic x rays or inelastically scattered electrons from very thin specimens or free surfaces to show the elemental distribution in the specimen. These experiments are difficult under high-resolution conditions because the collection and detection efficiencies for the signals have not yet been optimized, but they offer intriguing opportunities for examining the distribution of atomic species around lattice defects or on free surfaces. Figure 7 shows, for example, two images of magnesium-oxide cubes having a thin layer of nickel evaporated on two edges; figure 7b was produced with nickel Ka radiation in a field-emission scanning microscope. The cubes were about 10 nm in size, and the x-ray image shows the nickel layer to be roughly 2 nm thick. This corresponds to

around 1500 atoms of nickel in the irradiated volume. This image clearly shows the advantages of using small, high-current-density probes and ultrahigh vacuum systems.

The future

During the next decade we can expect that analytical electron microscopy will be applied to an increasing number of diverse problems in applied physics, materials science and solidstate chemistry. Particularly active research is expected on the mechanism of phase transformations at interphase interfaces in structural alloys and solid-state electronic devices and on the structure of catalytically active materials. It is likely that a significant fraction of future activity in high-resolution analytical microscopy will be concentrated in academic and industrial research centers, in view of its strong interdisciplinary nature and high capital cost for instrumentation.

Several laboratories are vigorously pursuing research in this field. In the longer term we can expect that new instruments capable of maintaining very clean environments in all operating modes will appear for use in high-resolution research on surface structure and compositions as well as inter-

nal microstructure. These instruments will, we can assume, incorporate field-emission electron sources, ultrahigh vacuum systems and increased accelerating voltages.

The author is indebted to his colleagues for discussions and for some of the results shown in this article, particularly to N.J. Zaluzec, D. M. Maher and J. M. Cowley. The support of the Division of Materials Sciences, US Department of Energy, and of the National Science Foundation is acknowledged.

References

- J. Hillier, R. F. Baker, J. Appl. Phys. 15, 663 (1944).
- Prc. Elec. Mic. Soc. Am., 29th Ann. Mtg., C. J. Arceneaux, ed., Clartor's Pub. Div. Baton Rouge, La. (1971). Articles by J. C. Russ, page 54; R. H. Duff, S. L. Bender, page 56; R. H. Geiss, W. A. Jesser, page 60.
- W. Kossel, G. Mollenstedt, Ann. Physik 5, 113 (1939).
- A. V. Crewe, J. Wall, L. M. Welter, J. Appl. Phys. 39, 5681 (1968).
- D. M. Maher, Scanning Electron Microscopy/1974, IIT Res. Inst., Chicago, Ill. (1974), page 215.
- R. W. Carpenter, J. Bentley, E. A. Kenik, Scanning Electron Microscopy/1977, IIT Res. Inst., Chicago, Ill. (1977), page 411.
- D. C. Joy, Scanning Electron Microscopy/1977/I, IIT Res. Inst., Chicago, Ill. (1977) page 1.
- J. J. Hren in Introduction to Analytical Electron Microscopy, J. J. Hren, J. I. Goldstein, D. C. Joy, eds, Plenum, N. Y. (1979), page 481.
- N. Oaskabe, K. Yagi, G. Honjo, Jap. J. Appl. Phys. 19, L309-L312 (1980).
- R. F. Egerton, Ultramicroscopy 3, 243 (1978).
- D. B. Williams, J. W. Edington, J. Microscopy 108, 113 (1976).
- D. C. Joy, D. M. Maher, Scanning Electron Microscopy/1977/I, IIT Res. Inst. Chicago, Ill. (1977).
- M. Isaacson, D. Johnson, Ultramicroscopy 1, 33 (1975).
- 14. N. J. Zaluzec, in reference 8, page 121.
- 15. J. Goldstein, in reference 8, page 83.
- D. M. Maher, Proc. Batelle Conf. on Microanalysis, Seattle, 1980 (in press).
- N. J. Zaluzec, Prc. Elec. Mic. Soc. of Amer., 38th Ann. Mtg., G. W. Bailey, eds., Clartor's Pub. Div., Baton Rouge, La. (1980) page 112.
- R. W. Carpenter, J. Bentley, Scanning Electron Microscopy/1979/I, SEM, Inc. AMF O'Hare, Ill., (1979) page 153.
- R. W. Carpenter, J. C. H. Spence, Acta Crystallographica (in press).
- P. M. Jones, G. M. Rackham, J. W. Steeds, Proc. Roy. Soc. London A354, 197 (1977).
- B. F. Buxton, J. A. Eades, J. W. Steeds, G. M. Rackham, Phil. Trans. Roy. Soc A281, 171 (1976).
- J. M. Cowley, Chemica Scripta 14, 33 (1978-79).
- 23. J. M. Cowley, S. Iijima, PHYSICS TODAT. 30, 32 (1977).